FDOI: 10.1002/ ((admi.201700336))

Full Paper

Giant Enhancement of Polarization and Strong Improvement of Retention in Epitaxial $Ba_{0.6}Sr_{0.4}TiO_3$-based Nanocomposites

OonJew Lee, *Ahmed Kursumovic*, *Zhenxing Bi*, *Chen-Fong Tsai*, *Haiyan Wang*, *and Judith L. MacManus-Driscoll**

Dr. O. J. Lee, Dr. A. Kursumovic, Prof. J. L. MacManus-Driscoll

Department of Materials Science and Metallurgy, University of Cambridge, 27 Charles Baggage Street, Cambridge CB3 0FS, United Kingdom

E-mail: jld35@cam.ac.uk

Dr. O. J. Lee

School of Fundamental Science, Universiti Malaysia Terengganu, 21030 Kuala Terengganu, Malaysia

E-mail: oonjew@umt.edu.my

Dr. Z. X. Bi

Department of Electrical and Computer Engineering, Texas A&M University, College Station, Texas 77843, USA

E-mail: zbi@us.ibm.com

Dr. C. F. Tsai, Prof. H. Y. Wang

Materials Science and Engineering Program, Texas A&M University, College Station, Texas 77843, USA

E-mail: hwang00@tamu.edu

Prof. H. Y. Wang

School of Materials Engineering, Purdue University, West Lafayette, IN 47907, USA

E-mail: hwang00@purdue.edu

In $Ba_{0.6}Sr_{0.4}TiO_3$ (BSTO)-based epitaxial nanocomposite films we demonstrate increased P_r values by up to a factor of 3 compared to standard BSTO films. A strongly reduced temperature coefficient of polarization retention was also obtained, i.e. 0.07% $°C^{-1}$ compared to 0.24% $°C^{-1}$. Piezo-poling with only marginal leakage current was also achieved up to 200 °C, the highest temperature studied. The origin of the improved performance was the incorporation of Sm_2O_3 nanopillars in the films which acted as stiff vertical nanoscaffolds, inducing a strong tetragonal distortion in the BSTO (up to 1.033(7) in terms of the *out-of-plane*/*in-plane* lattice dimensions). The films have comparable performance to industry-standard $Pb(Zr,Ti)O_3$ (PZT) films, at the same time as being Pb-free.

1. Introduction

A paradigm shift in ferroelectrics towards miniaturization has come about because of the considerable interest in low energy consumption and non-volatile nanoelectronics. The advances in the fabrication of ferroelectric structures in the nanometre range have brought to life new physical phenomena and encouraged unique combinations of functionalities.[1-3] $Ba_{0.6}Sr_{0.4}TiO_3$ (BSTO) is a ferroelectric of topical interest since it exhibits a wide variety of functional properties, including switchable polarization, piezoresponse, electro-optical behaviour, tunability and non-linear dielectric behaviour. It is also Pb-free. It could replace conventional microwave tunable devices made from III-V semiconductors which have drawbacks of slow response to input signal, high loss, and high operating voltage.[4] To date, $Pb(Zr,Ti)O_3$ (PZT) remains the industry standard material in nano- and micro-devices for exploiting the aforementioned functional properties.[5]

Reducing dimensions to the nanoscale is challenging for standard ferroelectrics. When the lateral and vertical dimensions of $(Ba,Sr)TiO_3$ and $BaTiO_3$ are downscaled to below 26 nm in

vertical thickness, or below 20 nm in nanowire lateral dimension, their functional properties are degraded compared to the bulk.[6-7] On the other hand, using vertically aligned nanocomposites films (of $BaTiO_3$-Sm_2O_3 and $Ba_{0.6}Sr_{0.4}TiO_3$-Sm_2O_3 compositions) containing lateral nanoscale features of sizes down to 10 nm, we have shown that size-limited property degradation is eliminated.[8-9] A key reason for this is that the interfaces of the ferroelectric nanostructures in the films are epitaxially coupled to a second scaffold phase in the film. In such films, there is strong vertical strain that causes a strong enhancement of Curie temperature,[8-9] enhanced dielectric tunability, reduced dielectric loss and leakage current[9] and, finally, enhanced saturation polarization.[2] On the other hand, in these promising nanocomposite ferroelectrics neither has the extent of polarization nor has the polarization retention been systematically studied.

$(Ba_{0.6}Sr_{0.4}TiO_3)_{1-x}$-$(Sm_2O_3)_x$, denoted henceforth as $(BSTO)_{1-x}(SmO)_x$, nanocomposite films with different thicknesses (300 nm, 600 nm and 1000 nm) were heteroepitaxially grown on $SrRuO_3$ (SRO)- buffered (00*l*) $SrTiO_3$ (STO) substrates by pulsed laser deposition (PLD). SmO is a cubic, non-polarizable phase with significantly greater stiffness (125 - 220 GPa) than BSTO (~80 GPa).[10-12]

2. Results and Discussion

First, we present the microstructures and structural information on the BSTO-SmO nanocomposites of most interest. These are for $(BSTO)_{1-x}(SmO)_x$ compositions with $x = 0.50$ and 0.75. An example cross-sectional TEM image for a $x = 0.75$ sample reveals the nanocolumnar structure obtained (**Figure 1**a,b). The $x = 0.75$ film was found to be the optimum composition for enhanced polarization owing to the greatest induced tetragonal distortion of the BSTO.[2, 9] Figure 1c shows a similar nanocolumnar matrix for $x = 0.50$. The lateral length scales for both x values are similar, i.e. 10 - 20 nm. The selected area electron diffraction (SAED) pattern for $x = 0.50$ (Figure 1d) shows 45° rotated growth of SmO on the (00*l*) SRO buffered STO substrate. The distinct spots show high epitaxial quality growth with

a low degree of misorientational spread.

XRD patterns in the supporting document (**Figure S1**) show the strong epitaxial growth of (00*l*) perovskite BSTO, cubic SmO, and pseudocubic SRO on (00*l*) perovskite STO substrates. The BSTO (002) peaks shift to lower angles (indicating *out-of-plane* lattice parameter expansion) with increasing SmO fraction, *x*. Hence, a systematic coherent tensile strain tuning in the vertical direction is achieved.[2] Based on Landau-Devonshire phenomenological theory, strain induced tetragonality is a crucial parameter influencing the polarization, tunability, Curie temperature, T_c and dielectric properties of a ferroelectric.[13] Herein, the tetragonality, *c/a* is defined as the ratio of *out-of-plane* lattice parameter, *c,* and *in-plane* lattice parameter, *a*.

We now study the ferroelectric properties of the nanocomposite films. **Figure 2**a shows remnant polarization, P_r, obtained from pulsed polarization measurements, also known as PUND measurements, versus tetragonality for the different films (more discussion and data on PUND measurements is shown later). In Table 1, supplementary information, we show *c* and *a* parameters, as well as *c/a,* and P_r for all the films of different *x* values and film thicknesses. We note in the middle region of Figure 2a, an unsual auxetic-like behavior (increase in *both c* and *a,* as shown in Table 1) is observed. This behaviour is related to how, upon cooling, the stiff SmO shrink and, in doing so, expand the BSTO matrix *in-plane,* as explained and modeled previously.[2]

Across the entire thickness range, a trend of increasing P_r with tetragonality is observed with a much more marked increase in P_r for the $x = 0.75$ samples. The highest P_r values are for the 1000 nm thickness films. P_r is 5.1 μC cm^{-2}, 5.8 μC cm^{-2} and 12.1 μC cm^{-2} for the x = 0.25, 0.50 and 0.75 films, consistent with the high *c/a* values of 1.006(6), 1.012(9) and 1.033(7), respectively. The P_r values for the $x = 0.75$ sample is 3 times higher than for plain BSTO ($x = 0$) of similar thickness (P_r = 3.9 μC cm^{-2}) and is approaching state-of-the-art, similar thickness epitaxial PZT films grown by PLD on Si (00*l*) with SRO and yttria-stablized

zirconia (YSZ) buffer layers, where P_r is 18.6 μC cm^{-2} from *P-E* loops measured at ±200 kV cm^{-1}.[14]

The *c/a* values obtained for the composite films are significantly larger than the plain BSTO (x = 0) films studied here and compared to literature BSTO films.[15] The highest value achieved was 1.033(7) for the x = 0.75 film of thickness 1000 nm. It is noted that in plain films a high level of tetragonality is maintained *only* up to a critical layer thickness of a few nanometres.[2, 9] On the other hand, in the nanocomposite films the different strain control mechanism means that there is no theoretical limit to strain control.[16] Indeed, *c/a* for our films *increases* with film thickness. For a given composition (or x value), the trend of increased tetragonality with film thickness is related to the fact that substrate control of the BSTO lattice parameters diminishes as the film thickness increases[9, 16] allowing the stiff second phase to have a full effect on the film strain state.

The highest *c/a* value of 1.033(7) (x = 0.75, 1000 nm film) obtained is significantly higher than *c/a* value reported for standard ferroelectric films previously, e.g. 1.019(9) for BTO.[17] Furthermore, the leakage is lower in the thicker films (see **Figure S2**, supporting information), consistent with earlier studies of BTO nanocomposite films.[18] The two factors of increased tetragonality and reduced leakage with film thickness explain why, for a given x value, P_r increases markedly with film thickness e.g. for x = 0.75, P_r is 5.8 μC cm^{-2} for a film thickness of 300 nm whereas it is 12.1 μCcm^{-2} for a film thickness of 1000 nm.

Figure 2b shows a schematic of the BSTO-SmO vertical interface heteroepitaxial matching depicting the strong tetragonal distortion induced in vertical nanocomposite films (thickness > ~50 nm) compared to plain, unstrained films which are cubic at room temperature. The enhanced *c* axis in the BSTO in the nanocomposite films originates from vertical lattice heteroepitaxy with the stiff nanoscaffold SmO phase. As already mentioned, the *a* lattice parameter is controlled by how the *in-plane* thermal contraction of the stiff SmO phase upon cooling the film acts on the film matrix.[2] In short, since the SmO is much stiffer

than the BSTO and it is epitaxially coupled to the BSTO, this leads either to *in-plane* contraction or expansion of the BSTO when the SmO either forms the nanocolumns (for $x <$ ~0.5) or matrix ($x >$ ~0.5), respectively.[2, 18] This is very different to conventional epitaxial films.

Figure 2c shows the *P-E* loops for the optimum composition, $x = 0.75$, films of different thickness. The P_r values of 6.0 μC cm^{-2}, 7.9 μC cm^{-2} and 13.2 μC cm^{-2} for the 300 nm, 600 nm and 1000 nm thicknesses, respectively, (marginally higher than the values obtained from the PUND measurements because PUND eliminates leakage and other spurious effects) correlate with the increasing *c*/*a* values of 1.023(9), 1.030(1) and 1.033(7), in the same way as the PUND-determined P_r values do. Comparing the *P-E* loop for the $x = 0.75$ sample to the pure BSTO film, ~3× higher nominal polarization values were achieved.

We now study the ferroelectric retention. High thermal and temporal retentions are critical for achieving unlimited switching without degradation of polarization but they are limited in many ferroelectric systems, e.g. in BSTO, $BaTiO_3$, $BiFeO_3$ and PZT because of depolarization, inhomogenous field distributions and defects.

In terms of thermal retention, thermal depolarization or back-switching of the poled state in the ferroelectric element occurs. The retention as a function of temperature is defined as:

$$R(T) = \left[1 - \frac{\Delta P_r(T)}{P_r(T_0)}\right] \times 100 \qquad (1)$$

where *R(T)* is the retention determined *via* PUND measurements. The change of remnant polarization, P_r can be described as $\Delta P_r(T) = P_r(T_0) - P_r(T)$ whereas $P_r(T_0)$ and $P_r(T)$ are the remnant polarizations measured at the initial temperature and elevated temperature, respectively.

In terms of temporal retention, *R(t)* is defined as:

$$R(t) = \left[1 - \frac{\Delta P_r}{P_r(0)}\right] \times 100 \qquad (2)$$

where ΔP_r is the change in remnant polarization during time, t.[19] With this definition, 100% retention in the ferroelectric element at any t will be observed if $\Delta P_r = P_r(0) - P_r(t)$, meaning that the state of polarization for the ferroelectric element has not changed. On the other hand, 0% retention will be obtained if $\Delta P_r = P_r(0)$ and $P_r(t) = 0$, i.e. the ferroelectric element is depoled entirely.

Figure 3 shows remnant polarization as a function of temperature for the nanocomposite films for $x = 0.25$ to $x = 0.75$, in comparison to plain BSTO films with 300 nm thickness obtained from both conventional *P-E* loops (Figure 3a) and PUND measurements (Figure 3b) as a function of temperature. The conventional hysteresis loops and PUND measurements complement each other. The former allows the charge or polarization developed from intrinsic polarization, parasitic capacitance and leakage contributions, to be determined when the electric field is applied to the ferroelectric film. The contribution of parasitic capacitance and leakage is inevitable if the measurement is carried out at an elevated temperature. The complementary PUND measurements, on the other hand, mitigate this problem since the remnant polarization is obtained through subtracting the non-switching polarization from the switching polarization, thus allowing intrinsic polarization to be determined.[20-21] Figure 3d shows a series of PUND pulses of 300 kV cm^{-1}, 1 ms pulse width and 1000 ms pulse delays for capturing both switching and non-switching polarizations.

P_r as a function of temperature (from *P-E* plots, Figure 3a) shows negative gradients at lower temperature and positive gradients at higher temperature (except for $x = 0.75$). The temperature at which there is transition of the gradient increases strongly with x. The positive gradients arise from thermally activated loss and the leakage build-up of free electric charges.[19, 22] For $x = 0$, we find only a positive gradient component to the plot. This is consistent with previously reported PLD grown BSTO films on MgO which were measured at

much lower temperatures, from 80 K to 220 K,[23] in order avoid the influence of parasitic interfacial capacitance. Such substrate-strained, very thin (50 nm) epitaxial films grown by RF-magnetron sputtering exhibited ferroelectric hysteresis up to 200 °C.[24] The substrate strain effect increases the T_c from the bulk, unstrained value of ~250 K (- 23 °C),[23] but *only* in very thin films where strain relaxation is limited.

The reduction of the positive gradient component of the graph for increasing x indicates that the reduced leakage scales inversely with tetragonality. The tetragonal distortion leads to an increase in the ferroelectric-paraelectric transition, T_c to well above room temperature (to ~500 °C),[9] without thickness limitation since the strain is not controlled by the substrate. Owing to the lower T_cs of standard plain unstrained BSTO films, the *P-E* loops in the literature were measured at low temperatures (typically < 300 K) where thermally activated leakage is not large. Here, leakage is low at much higher temperatures, i.e. *above* 250 K. The P_r as a function of temperature from PUND measurements, (Figure 3b) shows the intrinsic polarization of the BSTO-SmO films without the contribution of parasitic leakage. This is the reason that the positive gradient part is eliminated. Both Figure 3a and 3b show that the polarization is larger with increased x, while Figure 3b shows that P_r decays less rapidly with temperature with increasing x, indicating again the strong role of vertical strain on improving the ferroelectric behaviour.

Figure 3c shows a reduced decay of the thermal retention, *R(T)*, as x is increased. At 125 °C, *R(T)* values as high as 89% and 93% were obtained for the x = 0.50 and x = 0.75 films. These values are comparable to 89% measured in epitaxial $Pb(Zr_{0.52}Ti_{0.48})O_3$ films at the same temperature.[25] Both the x = 0.50 and x = 0.75 films maintain their retentions with 74% and 58% values measured at 375 °C. The x = 0.75 sample demonstrates a very low temperature coefficient of polarization retention of 0.07% $°C^{-1}$ (up to 375 °C) which compares to 0.24% $°C^{-1}$ for the x = 0 (plain BSTO) film. This temperature coefficient of polarization retention for the x = 0.75 sample is similar to the 0.09% $°C^{-1}$ value for $Pb(Zr,Ti)O_3$ films.[25]

Normally, as the structural dimensions of ferroelectrics are scaled down, polarization (depolarization), dielectric permittivity and Curie temperature are all reduced compared to bulk.[1] Indeed, depolarization effects are normally severe for nanoscale ferroelectrics.[26-28]

The enhanced thermal retention of polarization observed in the nanocomposites is consistent with the presence of a very high density ($Tb.inch^{-2}$) of vertical interfaces which can compensate the surface polarization charge between the electrodes and BSTO lattice. Hence, the depolarization field which influences the domain motion and degrades the polarization retention is strongly reduced. Also, the high density of vertical interfaces in the nanocomposites likely act as ferroelectric domain nucleation centres to produce vertical growth of 'needle-like' domains through the film, giving lateral expansion of domains within the BSTO with applied field. Furthermore, the lateral domain growth of BSTO is constrained by the vertical interfaces. Thus, these needle domains are pinned in a stable state when they are confined by the ~10 nm lateral dimensions in the nanostructured films (Figure 1). Our results are consistent with BSTO needle domains being stable, retaining ferroelectric polarization and giving rise to a strong improvement in thermal retention. They are unlike the needle domains in the compositionally graded $PbZr_{1-x}Ti_xO_3$ heterostructures which are labile under electrical excitation.[29]

The excellent retention shown in the nanocomposites is very beneficial for miniaturised devices incorporating ferroelectrics where retention after many switching cycles at elevated temperature presents a serious challenge. The x = 0.75 composition which has a low temperature coefficient of polarization, high retention and good depolarization stability. This contrasts to ferroelectrics nanostructures which do not involve having a supportive, strain-controlling scaffold phase as we do here, e.g. individual $BaTiO_3$ nanowires, $PbTiO_3$ nanotubes, $BaTiO_3$ and $BiFeO_3$ ultrathin films.[30-33]

Figure 4 demonstrates piezo phase contrast and effective piezo-displacement, d_{33}, of the x = 0.75 film of a 300 nm thickness film measured by piezoresponse force microscopy (PFM)

at room temperature (Figure 4a) and at 200 °C (Figure 4b). The sequential polarization switching with 10 kHz excitation frequency and ± 5 V AC modulating voltage superimposed on a ± 10 V DC bias was performed over various scan areas.[2] A clear contrast was observed indicating reversal of domain polarization at room temperature. The irreversible piezo-response with complete *out-of-plane* switching confirms the ferroelectric nature even up to 200 °C even though the contrast is slightly lower than at room temperature owing to the thermally activated leakage current. We recall that plain BSTO films of thicknesses above a few 10 nm are relaxed and exhibit a bulk T_c of only ~250 K (- 23 °C).[23]

The d_{33} curves for the x = 0.75 film (as shown in Figure 4c) display a characteristic 'butterfly' shape for the ferroelectric hysteresis, as expected, but with a reduced curve at 120 °C because of thermally activated leakage. Similar temperature dependent piezoresponse has been observed previously in (00*l*) oriented $PbZr_{0.2}Ti_{0.8}O_3$ (PZT) and epitaxial tetragonal $BiFeO_3$ films up to 400 °C and 180 °C, respectively.[34-35] The d_{33} values measured for the x = 0.75 film were 88.1 pm V^{-1} and 81.4 pm V^{-1} at room temperature and 120 °C, respectively. These d_{33} values are significantly higher than the room temperature d_{33} values for epitaxial $BaTiO_3$ films (54.0 pm V^{-1})[36] and $BaTiO_3$ nanowires (45.0 pm V^{-1}),[37] and are comparable to $BaZr_{0.2}Ti_{0.8}O_3$-$Ba_{0.7}Ca_{0.3}TiO_3$ films with (00*l*) orientation (67.8 pm V^{-1} – 85.9 pm V^{-1}).[38-39] They are also close to PZT films (~100 pm V^{-1} measured at 300 °C).[34] Thus, the PFM measurements confirm that the vertical strain effect in the composites retains the tetragonality in the BSTO up to at least 200 °C, the highest temperature studied here.

3. Conclusion

In summary, the structural and ferroelectric properties of 300, 600 and 1000 nm thickness epitaxial $(Ba_{0.6}Sr_{0.4}TiO_3)_{1-x}$-$(Sm_2O_3)_x$ nanocomposite films grown on $SrTiO_3$ were studied. The most beneficial ferroelectric properties were obtained for x = 0.75. Here, the film structure consisted of ~ 10 nm vertical nanocolumnar BSTO pillars in stiff Sm_2O_3 matrix. The

simply-made, self-assembled films give rise to very high tetragonality in the BSTO (*c*/*a* up to 1.033(7), compared to 0.995(3) in plain 1000 nm BSTO films). Consequently, very strongly improved thermal retention of polarization up to 375 °C was obtained. Piezo-poling with only marginal leakage current was also achieved up to 200 °C. In addition, depolarization from nanoscale size effects was overcome. Indeed, a three-fold increase in remnant polarization was obtained. Nanoscaffold vertical strain control in epitaxial nanocomposite thin films offers a novel and practical route to strongly improve nanoscale ferroelectric films.

4. Experimental Section

Deposition of (BSTO)$_{1-x}$(SmO)$_x$ Vertically Aligned Nanocomposites: (BSTO)$_{1-x}$(SmO)$_x$ were grown by PLD using a KrF excimer laser 248 nm. Five different composition (BSTO)$_{1-x}$(SmO)$_x$ (x = 0.00, 0.25, 0.50, 0.75 and 1.00) composite targets were synthesized *via* conventional mixing and solid state sintering. The substrate temperature, oxygen pressure and laser fluence were 800 °C, 20 Pa and approximately 2 J cm^{-2}, respectively. The films were made into metal-insulator-metallic oxide (MIM) test devices with sputtered coated Pt top circular electrodes (with a radius of 50 μm) and with SRO bottom electrodes. The 30 nm thick SRO bottom electrodes were deposited at 700 °C before the nanocomposite layers were grown.

Characterization: Crystallographic and microstructural investigations were carried out by high resolution X-ray diffraction (HRXRD), transmission electron microscopy (TEM) and scanning electron microscopy (SEM). Polarization-electric field hysteresis loops and remnant polarization, P_r, as a function of temperature were performed using a Radiant ferroelectric tester for both conventional polarization-electric field (*P*-*E*) loop and PUND (Positive Up Negative Down) measurements. In the PUND measurements a series of 5 pulses were applied at 300 kV cm^{-1} with pulse sequence of 0.1 ms to capture both switching and non-switching polarizations. The switching electric field of 300 kV cm^{-1} was relatively low (e.g. 9 V applied

on the BSTO-SmO nanocomposite films of 300 nm thickness). A delay of 1000 ms was set between the pulses. The initial pulse (Pulse 1) was applied to preset the film to the polarization stage and no measurement was made at this point. A second pulse (Pulse 2) was applied to switch the sign of polarization. After a 1000 ms pulse elapse, the film was left to relax, allowing the non-remnant polarization to be dissipated. A third pulse (Pulse 3) was then applied and the polarization measured without pre-switching. Fourth and fifth pulses (Pulse 4 and 5) were then applied, similar to Pulse 2 and 3 but with the opposite polarity. Piezoresponse force microscope (PFM) measurements were performed using an Agilent 5500 scanning probe microscope in PFM mode together with 3 lock-in amplifiers. The electrically biased conductive Atomic force microscopy (AFM) tip was used to detect the piezoresponse of the films through tip deflection.

Supporting Information

Supporting Information is available from the Wiley Online Library or from the author.

Acknowledgements

The authors acknowledge the support from the European Research Council (ERC) (Advanced Investigator Grant No. ERC-2009-AdG-247276-NOVOX), and EPSRC grant EP/K035282/1. The work conducted at Texas A&M University and Purdue University was supported by the U.S. National Science Foundation (DMR-1401266 (Texas A&M) and DMR-1643911 (Purdue)). The authors wish to acknowledge the assistance of M. Vickers and the use of the Chemical Database Service at Daresbury.

Received: ((will be filled in by the editorial staff))
Revised: ((will be filled in by the editorial staff))
Published online: ((will be filled in by the editorial staff))

References

[1] A. Gruverman, A. Kholkin, *Rep. Prog. Phys.* **2005**, *69*, 2443.

[2] J. MacManus-Driscoll, A. Suwardi, A. Kursumovic, Z. Bi, C.-F. Tsai, H. Wang, Q. Jia, O. J. Lee, *APL Mater.* **2015**, *3*, 062507.

[3] J. Varghese, R. W. Whatmore, J. D. Holmes, *J. Mater Chem. C* **2013**, *1*, 2618.

[4] B. York, in Multifunctional Adaptive Microwave Circuits and Systems (Eds: M. Steer, W. D. Palmer), Scitech Publishing, Raleigh, NC, 2009, Ch. 4.

[5] M. Alguero, J. M. Gregg, L. Mitoseriu, Nanoscale Ferroelectrics and Multiferroics: Key Processing and Characterization Issues, and Nanoscale Effects, Wiley, West Sussex, UK 2016.

[6] K. Abe, S. Komatsu, N. Yanase, K. Sano, T. Kawakubo, *Jpn. J. Appl. Phys.* **1997**, *36*, 5575.

[7] J. Hong, D. Fang, *Appl. Phys. Lett.* **2008**, *92*, 12906.

[8] S. A. Harrington, J. Zhai, S. Denev, V. Gopalan, H. Wang, Z. Bi, S. A. T. Redfern, S.-H. Baek, C. W. Bark, C.-B. Eom, Q. Jia, M. E. Vickers, J. L. MacManus-Driscoll, *Nat. Nanotechnol.* 2011, 6, 491.

[9] O. Lee, S. A. Harrington, A. Kursumovic, E. Defay, H. Wang, Z. Bi, C.-F. Tsai, L. Yan, Q. Jia, J. L. MacManus-Driscoll, *Nano Lett.* **2012**, *12*, 4311.

[10] T.-H. Fang, W.-J. Chang, C.-M. Lin, L.-W. Ji, Y.-S. Chang, Y.-J. Hsiao, *Mater. Sci. Eng.: A* **2006**, *426*, 157.

[11] D. S. D. Gunn, N. L. Allan, J. A. Purton, *J. Mater. Chem. A* **2014**, *2*, 13407.

[12] R. G. Munro, *J. Res. Natl. Inst. Stand. Technol.* **2004**, *109*, 497.

[13] D. G. Schlom, L.-Q. Chen, C.-B. Eom, K. M. Rabe, S. K. Streiffer, J.-M. Triscone,

Annu. Rev. Mater. Res. **2007**, *37*, 589.

[14] M. D. Nguyen, H. N. Vu, D. H. Blank, G. Rijnders, *Adv. Nat. Sci.: Nanosci. Nanotechnol.* **2011**, *2*, 015005.

[15] A. L. Campbell, R. R. Biggers, G. Subramanyam, G. Kozlowski, R. A. Kleismit, H. N. Zate, S. C. Hopkins, B. A. Glowacki, B. D. Riehl, T. L. Peterson, *Nanotechnology* **2008**, *19*, 485704.

[16] J. L. MacManus-Driscoll, P. Zerrer, H. Wang, H. Yang, J. Yoon, A. Fouchet, R. Yu, M. G. Blamire, Q. Jia, *Nat. Mater.* **2008**, *7*, 314.

[17] M. Jimi, T. Ohnishi, K. Terai, M. Kawasaki, M. Lippmaa, *Thin solid films* **2005**, *486*, 158.

[18] J. L. MacManus-Driscoll, A. Suwardi, H. Wang, *MRS Bull.* **2015**, *40*, 933.

[19] B. Sharma, S. Vogel, P. Prentky, *Ferroelectrics* **1973**, *5*, 69.

[20] Y. So, D. Kim, T. Noh, J.-G. Yoon, T. Song, *J. Korean Phys. Soc.* **2005**, *46*, 40.

[21] S. Zhukov, Y. A. Genenko, H. von Seggern, *J. Appl. Phys.* **2010**, *108*, 014106.

[22] A. Sharma, A. Teverovsky, Preliminary Evaluation of Data Retention Characteristics for Ferroelectric Random Access Memories (FRAMs). NASA Goddard Space Flight Center Report 2001, 1-4.

[23] A. Lookman, R. Bowman, J. Gregg, J. Kut, S. Rios, M. Dawber, A. Ruediger, J. Scott, *J. Appl. Phys.* **2004**, *96*, 555.

[24] K. Abe, N. Yanase, K. Sano, M. Izuha, N. Fukushima, T. Kawakubo, *Integr. Ferroelectr.* **1998**, *21*, 197.

[25] Y. Nomura, T. Tachi, T. Kawae, A. Morimoto, *Phys. Status Solidi B* **2015**, *252*, 833.

[26] M. Dawber, P. Chandra, P. Littlewood, J. Scott, *J. Phys.: Condens. Matter* **2003**, *15*, L393.

[27] C. Lichtensteiger, S. Fernandez-Pena, C. Weymann, P. Zubko, J.-M. Triscone, *Nano Lett.* **2014**, *14*, 4205.

[28] A. Stamm, D. Kim, H. Lu, C. Bark, C. Eom, A. Gruverman, *Appl. Phys. Lett.* **2013**, *102*, 092901.

[29] J. Agar, A. Damodaran, M. Okatan, J. Kacher, C. Gammer, R. Vasudevan, S. Pandya, L. Dedon, R. Mangalam, G. Velarde, S. Jesse, *Nat. Mater.* **2016**, *15*, 549.

[30] J. J. Urban, J. E. Spanier, L. Ouyang, W. S. Yun, H. Park, *Adv. Mater.* **2003**, *15*, 423.

[31] J. E. Spanier, A. M. Kolpak, J. J. Urban, I. Grinberg, L. Ouyang, W. S. Yun, A. M. Rappe, H. Park, *Nano Lett.* **2006**, *6*, 735.

[32] H. Choi, Y. Kim, S. Hong, T. H. Sung, H. Shin, K. No, *Phys. Status Solidi Rapid Res. Lett*. **2011**, *5*, 289.

[33] J. Zhao, H. Lu, J. Sun, B. Shen, *Phys. B* **2012**, *407*, 2258.

[34] B. Bhatia, J. Karthik, D. Cahill, L. Martin, W. King, *Appl. Phys. Lett.* **2011**, *99*, 173103.

[35] K.-T. Ko, M. H. Jung, Q. He, J. H. Lee, C. S. Woo, K. Chu, J. Seidel, B.-G. Jeon, Y. S. Oh, K. H. Kim, *Nat. Commun.* **2011**, *2*, 567.

[36] I.-D. Kim, Y. Avrahami, H. L. Tuller, Y.-B. Park, M. J. Dicken, H. A. Atwater, *Appl. Phys. Lett.* **2005**, *86*, 192907.

[37] Z. Zhou, H. Tang, H. A. Sodano, *ACS Appl. Mater. Interfaces* **2013**, *5*, 11894.

[38] B. Luo, D. Wang, M. Duan, S. Li, *Appl. Phys. Lett.* **2013**, *103*, 122903.

[39] A. Piorra, A. Petraru, H. Kohlstedt, M. Wuttig, E. Quandt, *J. Appl. Phys.* **2011**, *109*, 104101.

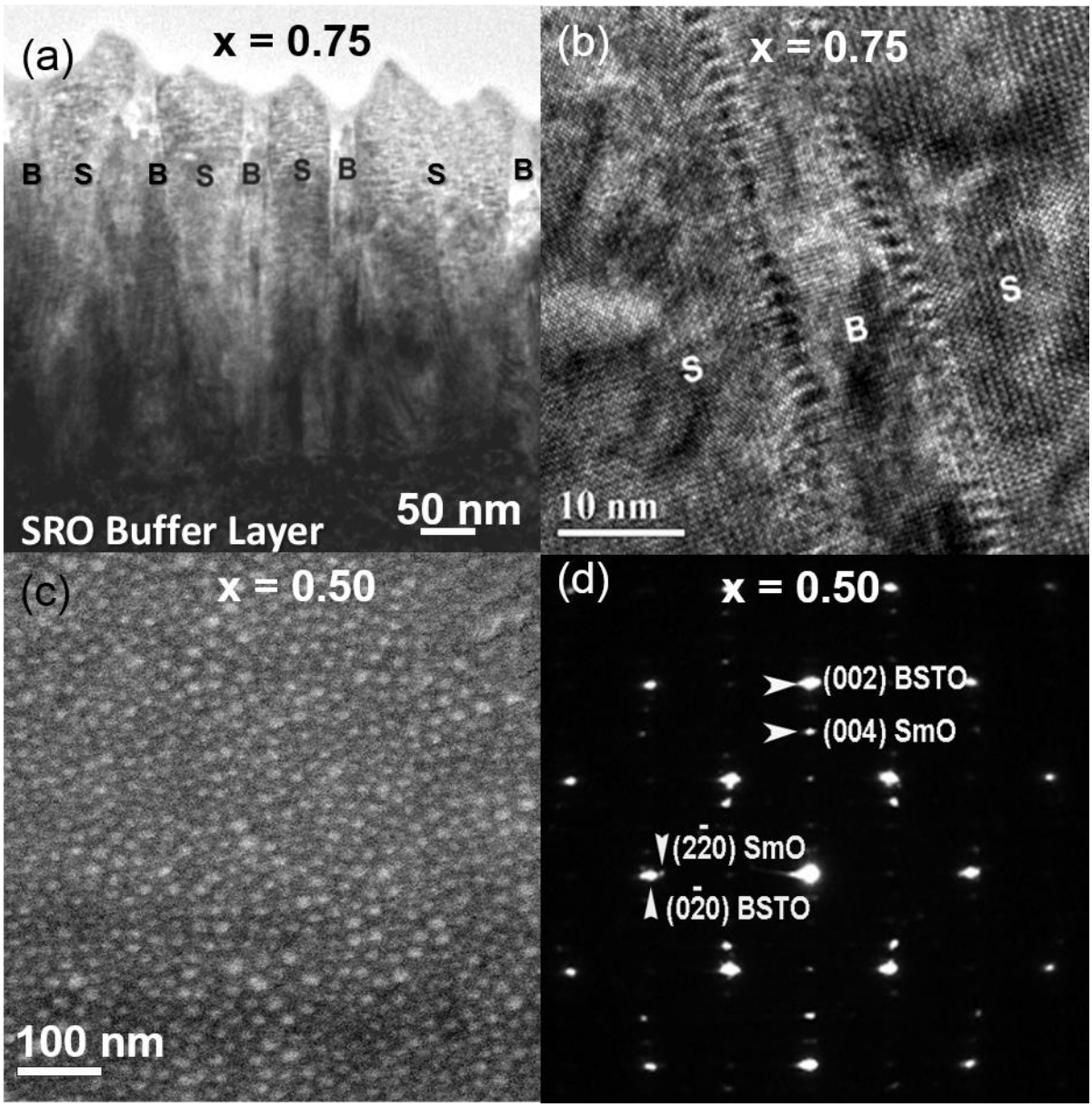

Figure 1. Self-assembled vertical aligned, epitaxial nanocomposite BSTO-SmO films. (a) TEM cross section of x = 0.75 film. (b) Clean interfaces between the BSTO and SmO phases in x = 0.75 film (represented by B and S, respectively) with Moire fringes observed. (c) SEM plan-view image of x = 0.50 film. (d) Selected area diffraction pattern of x = 0.50 film illustrating the *in-plane* heteroepitaxy between the BSTO and SmO phases.

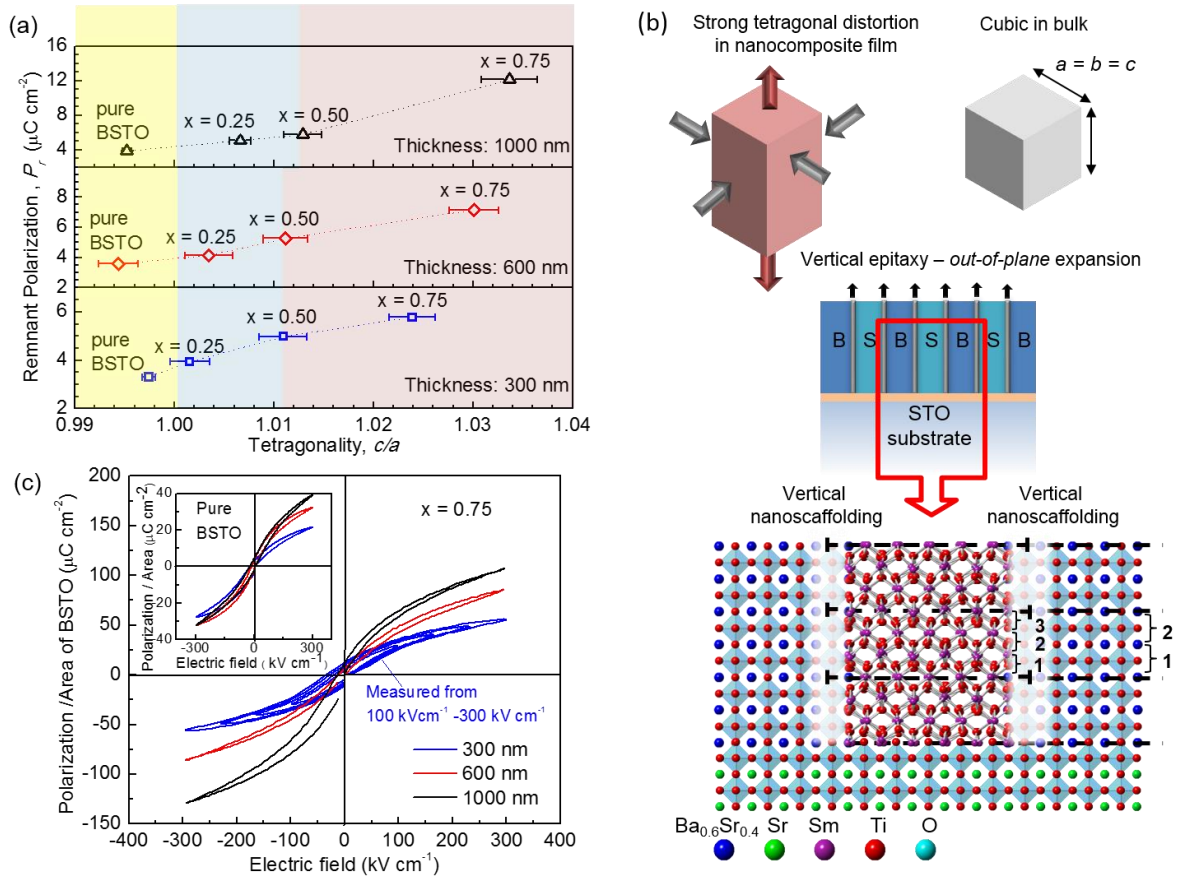

Figure 2. Ferroelectric polarizations and tetragonalities of the BSTO-SmO films. (a) Remnant polarization, P_r, versus tetragonality, *c/a*, of BSTO-SmO films, (b) Schematic of BSTO lattice under tetragonal distortion, and (c) polarization-electric field, *P-E*, hysteresis loops for x = 0.75 films (measured from 100 kV cm^{-1} to 300 kV cm^{-1}) for 300 nm, 600 nm, and 1000 nm thicknesses compared to pure BSTO film of the same thickness (inset).

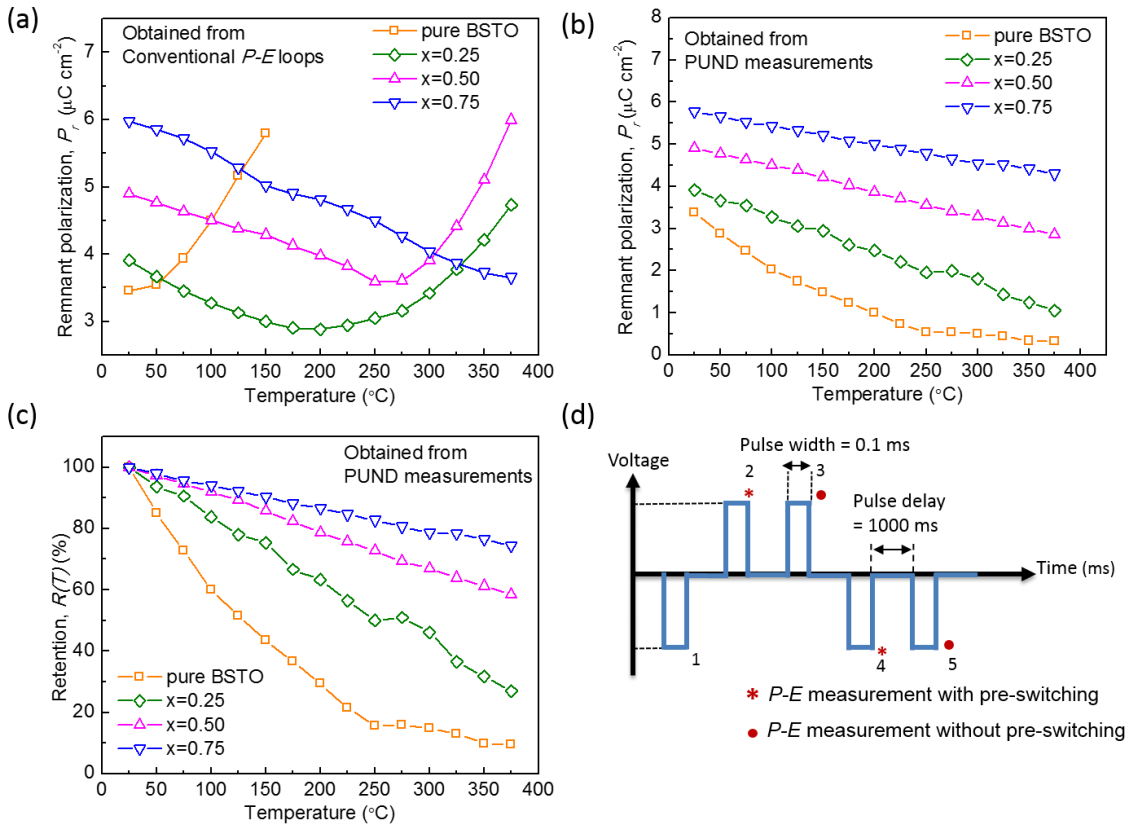

Figure 3. Temperature dependence of remnant polarization, P_r, and temperature dependent retention, *R(T)%* for BSTO-SmO films of 300 nm thickness. P_r *a*s a function of temperature, obtained from (a) conventional *P-E* loops, and (b) PUND measurement, (c) *R(T)%* as a function of temperature, and (d) a series of 5 pulses used in the PUND measurements. For all films, the P_r values are calculated using the film area under circular electrodes with a radius of 50 μm.

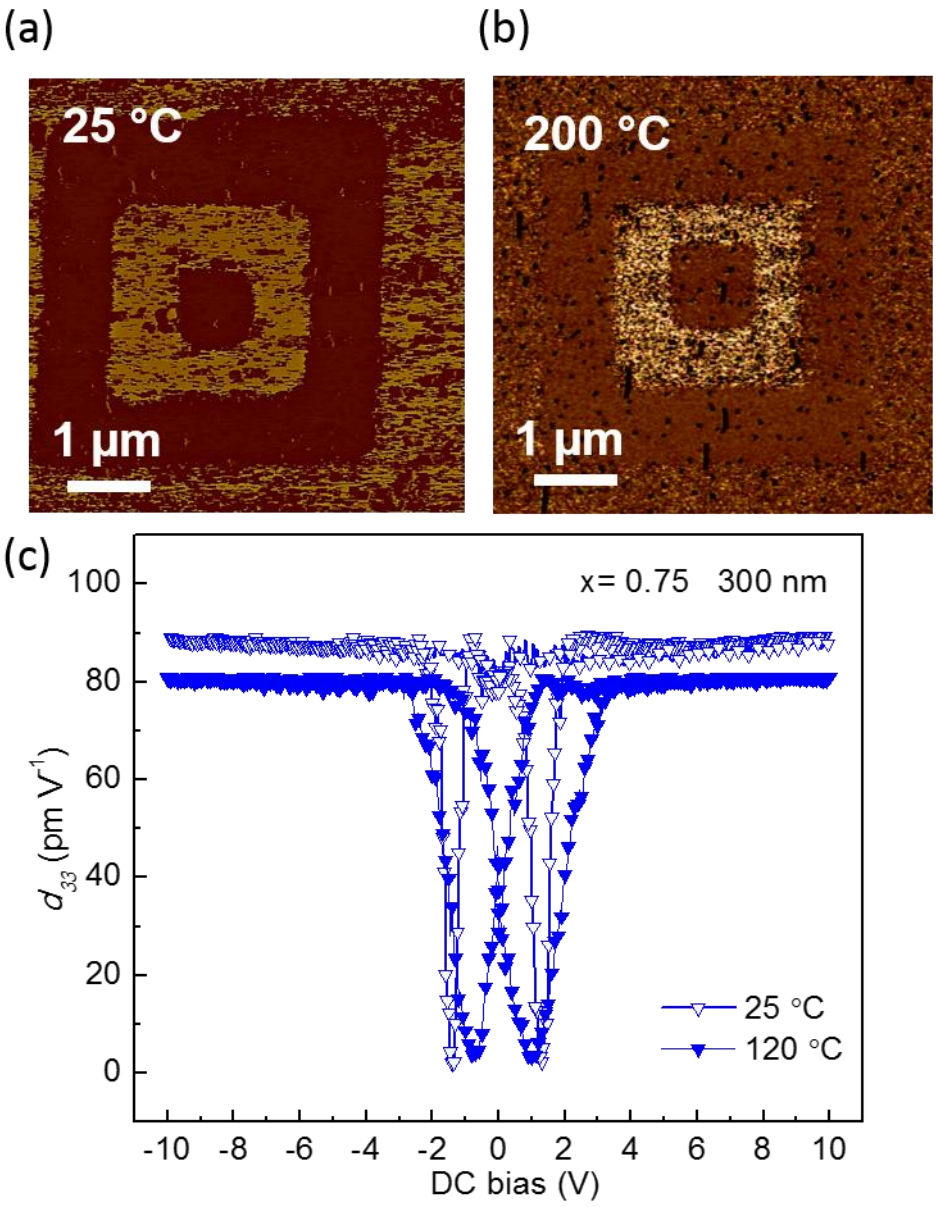

Figure 4. Piezo-hysteresis responses of BSTO-SmO, x = 0.75, film of 300 nm thickness. (a) PFM phase image with multiple poling measured at room temperature (25 °C) and (b) PFM phase image on the same spot, but measured at 200 °C. (c) Piezo-displacement, d_{33} measured at 25 °C and 120 °C. Both multiple poling domain configurations developed in the areas of 8 × 8, 5 × 5 and 2 × 2 μm^2 with applied DC bias of ± 10 V at excitation frequency of 10 kHz.

Table of Contents Graphic and Synopsis

$Ba_{0.6}Sr_{0.4}TiO_3$ (BSTO) - Sm_2O_3, vertical heteroepitaxial films with high induced tetragonality. Piezoresponse force microscopy (PFM) measurements show that ferroelectricity is retained to at least 200 °C. In addition, ~3× increased remnant polarization is obtained as well as a strongly reduced temperature coefficient of polarization retention.

Keywords: vertically aligned nanocomposites, ferroelectricity, polarization, retention, tetragonality

OonJew Lee, *Ahmed Kursumovic*, *Zhenxing Bi*, *Chen-Fong Tsa*, *Haiyan Wang*, *and Judith L. MacManus-Driscoll**

Giant Enhancement of Polarization and Strong Improvement of Retention in Epitaxial $Ba_{0.6}Sr_{0.4}TiO_3$-based Nanocomposites

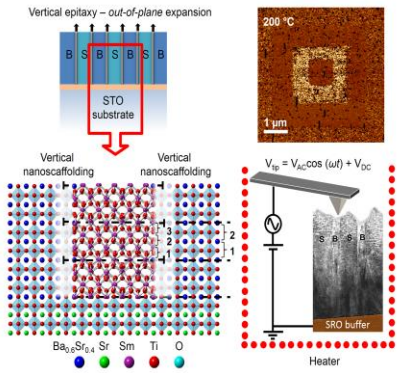

Supporting Information

Giant Enhancement of Polarization and Strong Improvement of Retention in Epitaxial $Ba_{0.6}Sr_{0.4}TiO_3$-based Nanocomposites

OonJew Lee, *Ahmed Kursumovic*, *Zhenxing Bi*, *Chen-Fong Tsa*, *Haiyan Wang*, *and Judith L. MacManus-Driscoll**

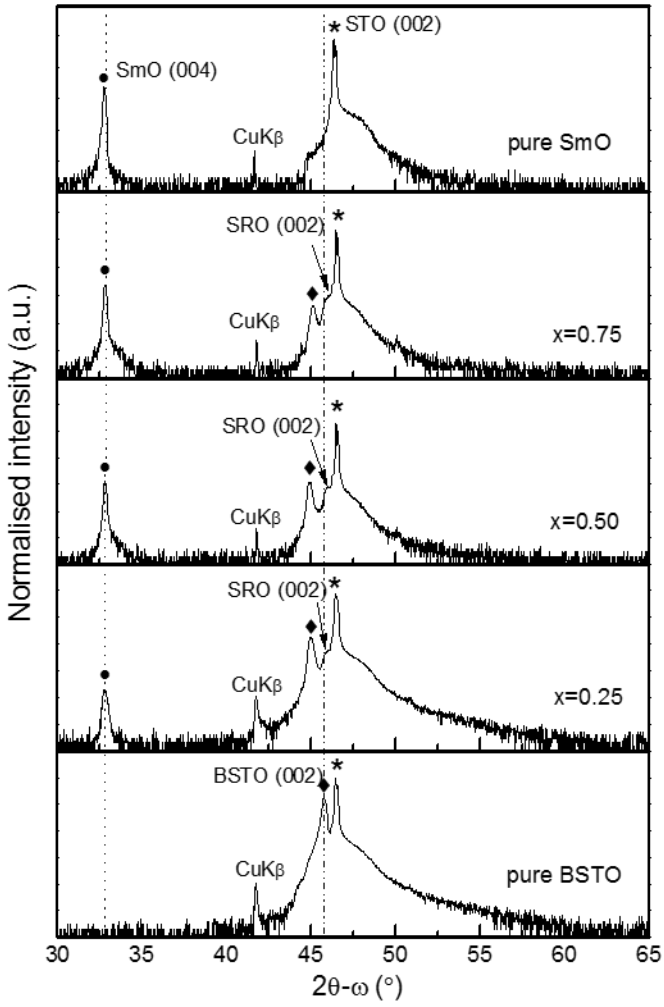

Figure S1. 2θ-ω XRD patterns of BSTO-SmO nanocomposite films around the (002) SRO/STO reflections.

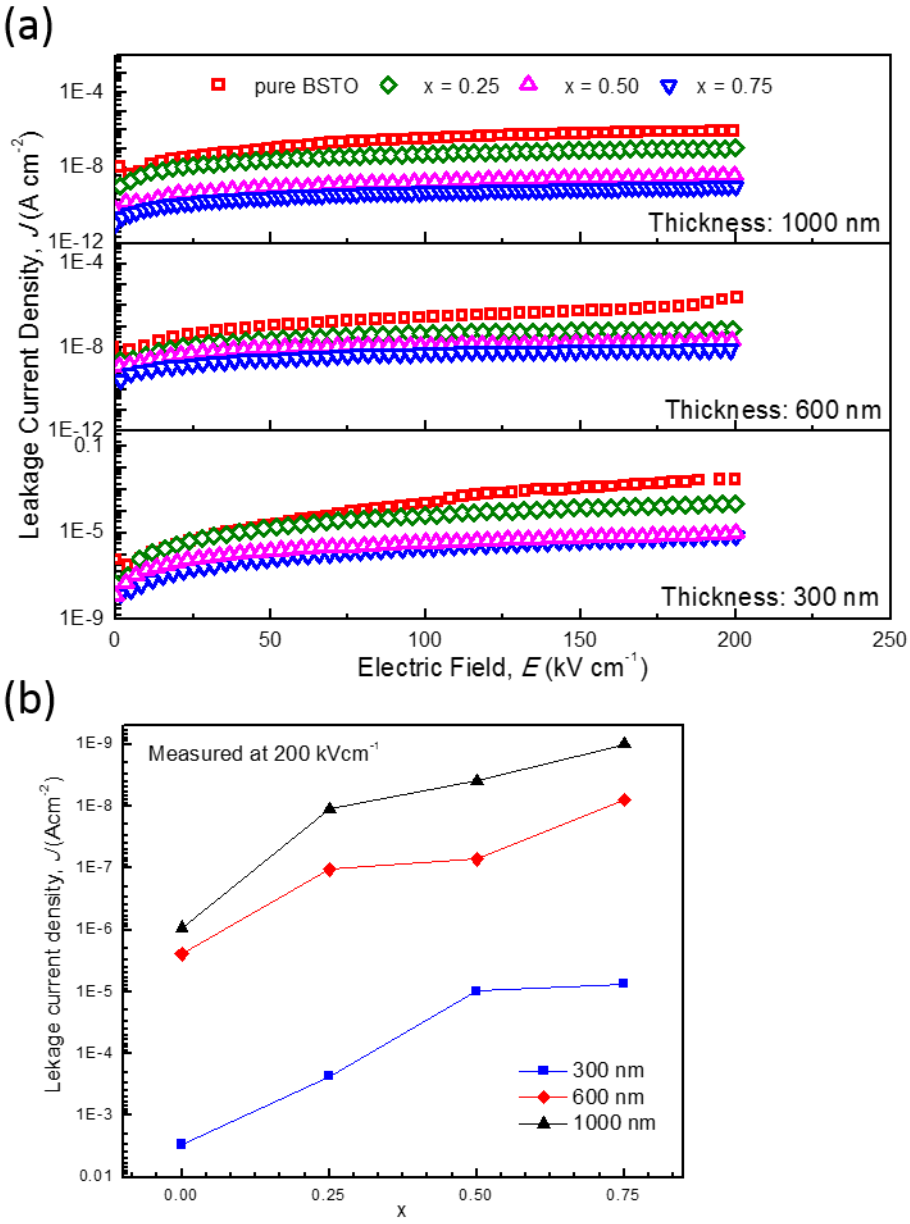

Figure S2. (a) Leakage current density-electric field, *J-E* characteristics of BSTO-SmO films of 300 nm, 600 nm and 1000 nm thickness, and (b) leakage current density measured at 200 kV cm^{-1} as a function of *x*.

Table 1. *c*-, *a*- lattice parameters and tetragonalities, *c/a*, of the BSTO phase and P_r values (determined from PUND measurements) for the different BSTO-SmO films of 300, 600 and 1000 nm thickness.

$BSTO_{1-x}SmO_x$	Thicknesses (nm)	*c*-lattice parameters (nm)	*a*-lattice parameters (nm)	Tetragonality, c/a	P_r ($\mu C/cm^2$)
Bulk BSTO (JCPDS 34-0411)	-	0.3965	0.3965	1.0000	-
Pure BSTO	300	0.3962 ± 3.5 e-5	0.3972 ± 6.4 e-4	0.9974 ± 6.8 e-4	3.3
$x = 0.25$	300	0.4016 ± 9.0 e-4	0.4010 ± 1.1 e-3	1.0016 ± 2.0 e-3	3.9
$x = 0.50$	300	0.4044 ± 1.3 e-3	0.4000 ± 1.1 e-3	1.0110 ± 2.4 e-3	4.9
$x = 0.75$	300	0.4032 ± 1.1 e-3	0.3938 ± 1.2 e-3	1.0239 ± 2.3 e-3	5.8
Pure BSTO	600	0.3958 ± 3.1 e-4	0.3981 ± 4.0 e-3	0.9944 ± 4.3 e-3	3.6
$x = 0.25$	600	0.4027 ± 1.0 e-3	0.4013 ± 1.4 e-3	1.0034 ± 2.4 e-3	4.2
$x = 0.50$	600	0.4048 ± 1.3 e-3	0.4004 ± 8.5 e-4	1.0112 ± 2.2 e-3	5.3
$x = 0.75$	600	0.4034 ± 7.2 e-4	0.3917 ± 1.8 e-3	1.0301 ± 2.5 e-3	7.2
Pure BSTO	1000	0.3961 ± 2.1 e-4	0.3978 ± 2.8 e-4	0.9953 ± 4.9 e-4	3.9
$x = 0.25$	1000	0.4043 ± 8.0 e-4	0.4017 ± 2.6 e-4	1.0066 ± 1.1 e-3	5.1
$x = 0.50$	1000	0.4060 ± 4.5e-4	0.4007 ± 1.4 e-3	1.0129 ± 1.9 e-3	5.8
$x = 0.75$	1000	0.4050 ± 1.3e-3	0.3918 ± 2.7 e-3	1.0337 ± 4.0 e-3	12.1